Numerical Modeling in Induction Heating for Axisymmetric Geometries

C. Chaboudez, S. Clain, R. Glardon, D. Mari, J. Rappaz, and M. Swierkosz

Abstract—**This paper deals with numerical simulation of induction heating for axisymmetric geometries. A mathematical model is presented, together with a numerical scheme based on the Finite Element Method. A numerical simulation code was implemented using the model presented in this paper. A comparison between results given by the code and experimental measurements is provided.**

I. Introduction

INDUCTION heating is widely used in today's industry, in operations such as metal hardening, preheating for forging operations, or brazing [3]. It is a complex process, involving both electromagnetic and thermal phenomena. Since the design and the investigation of an induction heating system usually relies upon a series of tedious, expensive and long experiments, numerical simulation can be a valuable help in this field [4]–[20]. The authors previously dealt with induction heating of long workpieces, obtaining encouraging results [1], [2].

In this paper, we deal with numerical simulation of induction heating with a rotational symmetry. The aim of our research was to elaborate mathematical and numerical models, and to implement efficient numerical codes for the simulation of induction heating. Several experimental measurements have been carried out by the company AMYSA Yverdon S.A. in order to validate the results provided by our numerical simulation codes. In this paper, we shall first present the model and the numerical methods used for the code. Next, we shall describe the experiments performed and compare them to the numerical simulation results. Finally, conclusions will be drawn.

Numerical simulation of induction heating clearly involves two coupled phenomena: electromagnetism and heating. An efficient eddy current computation has to be performed in order to obtain the source term to be plugged into the heat equation.

As far as eddy current computation is concerned, we opted for a formulation in magnetic potential to solve the electromagnetic problem. We chose to prescribe voltage in the conductors, rather than the total current, which was dictated by the commonly used generator setup. For computational efficiency reasons, we limited our scope to sinusoidal voltages, which allowed us to solve several times a steady-state equation rather than an evolutive one. In fact, the experience previously gathered [1] shows that the shape of the voltage has a limited importance from the energetic point of view, while solving a steady-state equation rather than an evolutive one allows significant savings of computation time. The physical properties of the heated materials may vary with the temperature. The possibility of using several coils and several voltage generators working at different frequencies has been taken into account.

Manuscript received December 6, 1994; revised May 14, 1996. This work was supported by the Swiss "Nationaler Energie-Forschungs-Fonds."

C. Chaboudez, R. Glardon, and D. Mari are with Amysa-Yverdon S.A., 1400 Yverdon-les-Bains, Switzerland.

S. Clain, J. Rappaz, and M. Swierkosz are with the Department of Mathematics, Swiss Federal Institute of Technology, 1015 Lausanne, Switzerland.

Publisher Item Identifier S 0018-9464(97)00084-8.

II. The Model

We consider an induction heating system consisting of one or several inductors and workpieces, all of them with an axial symmetry (Fig. 1). It will be assumed that there are neither displacement currents nor surface currents, and that the inductors are supplied with a sinusoidal current having a prescribed voltage. We consider that the properties of the materials used, i.e., the magnetic permeability μ, the electric conductivity σ, the thermal conductivity λ, the density ρ, and the specific heat C_p may depend on the temperature.

For the sake of simplicity, we describe a model consisting of one workpiece and one coil. Nevertheless, all our considerations remain valid for induction setups including several workpieces and coils. We shall denote by Ω_0 the workpiece to be heated, and by $\Omega_1, \Omega_2, \cdots, \Omega_n$ the windings of the coil. $\Omega = \Omega_0 \cup \Omega_1 \cup \Omega_2 \cup \cdots \Omega_n$ is the whole set of conductors (i.e., the coil and the workpiece). We suppose that a total sinusoidal voltage $v_k e^{i\omega t}$ (possibly zero) is imposed in the conductor Ω_k. The choice of imposing the total voltage rather than the total current is motivated by the setup of generators used in induction heating, which generally allows better control of the voltage than the current.

A. Mathematical Model

In order to obtain the mathematical model, we shall start from Maxwell's equations and Ohm's law, with displacement currents neglected. We denote by $\boldsymbol{E}$ the electric field, by $\boldsymbol{H}$ the magnetic field, by $\boldsymbol{B}$ the magnetic induction, by $\boldsymbol{j}$ the current density, and by ν the magnetic reluctivity, i.e., the inverse of the magnetic permeability μ. Maxwell's equations provide the following system:

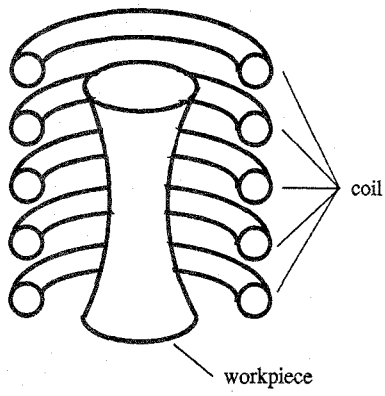

Fig. 1. An induction heating setup with axial symmetry.

$$\text{div } \boldsymbol{B} = 0 \tag{2.1}$$

$$\boldsymbol{curl}\ \boldsymbol{E} = -\frac{\partial \boldsymbol{B}}{\partial t} \tag{2.2}$$

$$\boldsymbol{curl}\ \boldsymbol{H} = \boldsymbol{j} \tag{2.3}$$

$$\nu \boldsymbol{B} = \boldsymbol{H} \tag{2.4}$$

valid in the whole space. From Ohm's law, we get

$$\boldsymbol{j} = \sigma \boldsymbol{E} \tag{2.5}$$

inside the conductors,

$$\boldsymbol{j} = 0 \tag{2.6}$$

in the space outside the conductors.

Let $(\vec{e}_r, \vec{e}_\theta, \vec{e}_z)$ be the natural tangent system associated with the cylindrical coordinates (r, θ, z) such that the Oz-axis is the symmetry axis of the induction heating system. The current density is supposed to be in the form $\boldsymbol{j} = j(r, z)e^{i\omega t}\vec{e}_\theta$, where ω is the angular frequency of the current and t is the time. It is also assumed that the components of the fields $\boldsymbol{H}$, $\boldsymbol{E}$, $\boldsymbol{B}$ in the system $(\vec{e}_r, \vec{e}_\theta, \vec{e}_z)$ depend only on r, z, and t (not on θ). Equation (2.3) yields then that $\boldsymbol{H}(r, z)$ is of the form

$$\boldsymbol{H}(r, z) = (H_r(r, z)\vec{e}_r + H_z(r, z)\vec{e}_z)e^{i\omega t}. \tag{2.7}$$

Let $\boldsymbol{A}$ be a magnetic vector potential, i.e., a magnetic field satisfying

$$\boldsymbol{B} = \boldsymbol{curl}\ \boldsymbol{A}. \tag{2.8}$$

We take $\boldsymbol{A}$ to be divergence-free (Coulomb gauge). Using (2.4), (2.7), and (2.8), it can be shown that $\boldsymbol{A}$ may be expressed in terms of a continuous scalar potential ϕ depending only on r and z:

$$\boldsymbol{A} = e^{i\omega t}\phi(r, z)\vec{e}_\theta.$$

Using the notation $\boldsymbol{B}(r, z) = (B_r(r, z)\vec{e}_r + B_z(r, z)\vec{e}_z)e^{i\omega t}$, we get from (2.8)

$$B_r = -\frac{\partial \phi}{\partial z}$$

$$B_z = \frac{1}{r}\frac{\partial (r\phi)}{\partial r}. \tag{2.9}$$

From (2.2) we have

$$\boldsymbol{curl}\ \boldsymbol{E} + i\omega \boldsymbol{B} = 0$$

and using (2.8) we get that

$$\boldsymbol{curl}\ (\boldsymbol{E} + i\omega \boldsymbol{A}) = 0.$$

In any conductor (workpiece or inductor), Ohm's law (2.5) holds, and therefore

$$\boldsymbol{curl}\ ((\sigma^{-1}j + i\omega\phi)\vec{e}_\theta) = 0.$$

It follows that $(\sigma^{-1}rj + i\omega r\phi)$ is a constant in each connected component of a conductor, and we can show that this constant is equal to $v_k/2\pi$, where v_k is the total voltage imposed in the conductor. Finally, we will have in any conductor Ω_k

$$j = \sigma\left(-i\omega\phi + \frac{v_k}{2\pi r}\right). \tag{2.10}$$

Using (2.3), (2.4), (2.9), and (2.10), we get inside the conductors (coils and workpieces) the equation

$$-\left(\frac{\partial}{\partial r}\left(\frac{\nu}{r}\frac{\partial (r\phi)}{\partial r}\right) + \frac{\partial}{\partial z}\left(\nu\frac{\partial \phi}{\partial z}\right)\right) + i\sigma\omega\phi = \sigma\frac{v_k}{2\pi r}. \tag{2.11}$$

In a similar way, the relations (2.3), (2.4), (2.6), and (2.9) combined together provide the following equation in the space outside the conductors:

$$\frac{\partial}{\partial r}\left(\frac{\nu}{r}\frac{\partial (r\phi)}{\partial r}\right) + \frac{\partial}{\partial z}\left(\nu\frac{\partial \phi}{\partial z}\right) = 0. \tag{2.12}$$

Since there are no surface currents, the following interface condition holds at the boundary of any conductor:

$$\left[\frac{\nu}{r}\left(\frac{\partial (r\phi)}{\partial r}n_r + \frac{\partial (r\phi)}{\partial z}n_z\right)\right] = 0 \tag{2.13}$$

where $[\psi]$ denotes the jump of a function ψ at the boundary of the conductor and $\boldsymbol{n} = n_r\vec{e}_r + n_z\vec{e}_z$ is the normal vector on the interface.

For the electromagnetic computations, we shall consider a rectangular box in the (r, z)-plan, surrounding the induction heating system, and big enough for the magnetic field to be weak at the boundaries of the box (Fig. 2).

The Biot–Savart hypothesis implies that the field $\boldsymbol{B}$ behaves like $1/(r^3 + z^3)$ far from the conductors. For big values of r, the behavior of ϕ can be considered to be similar to $1/r^2$. Therefore, on the boundaries of the box which are parallel to the symmetry axis, we impose a so-called Robin condition [21, p. 162]

$$\frac{\partial (r\phi)}{\partial r} + \phi = 0. \tag{2.14}$$

For those boundaries of the box which are perpendicular to the symmetry axis, a Robin-like condition is difficult to enforce. Instead, we set the condition

$$\frac{\partial (r\phi)}{\partial z} = 0 \tag{2.15}$$

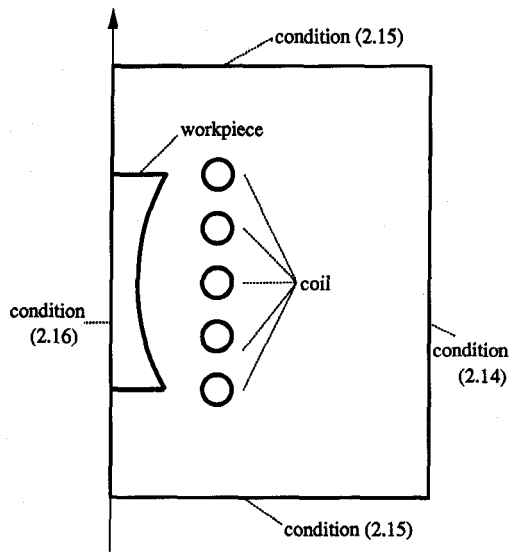

Fig. 2. Cross section of an induction heating setup together with the boundary conditions.

which stems from the assumption that the radial component of the magnetic field is close to zero on these boundaries.

Finally, the natural symmetry condition along the revolution axis is

$$\phi = 0. \tag{2.16}$$

To sum up, the electromagnetic model to be solved consists of (2.11) and (2.12), together with the interface condition (2.13), the boundary conditions (2.15) and (2.14), as well as the symmetry condition (2.16).

In order to study the thermal effects of the electromagnetic phenomena, the above model will be coupled with the heat equation. We shall assume that the workpieces do not interact thermally. This assumption will allow us to solve the heat equation individually for each workpiece. The Joule effect power term is $\sigma^{-1}|j_m|^2$, where j_m is the mean current density, equal to $j/\sqrt{2}$ in our case. The value of j is directly obtained by (2.10). Therefore, the equation to be solved in order to get the temperature field in the workpiece is

$$\rho C_p \frac{\partial T}{\partial t} - (\lambda \nabla T) = \frac{\sigma}{2}\left| \left(-i\omega\phi + \frac{v_k}{2\pi r} \right) \right|^2. \tag{2.17}$$

This equation is completed by the following radiation condition on the boundary of the workpiece, which is justified if the workpiece is convex and there is a large difference in temperature between the workpiece and the surrounding space:

$$\lambda \frac{\partial T}{\partial n} + \alpha(T^4 - T_{amb}^4) = 0 \tag{2.18}$$

where α is the product of the Stefan–Boltzmann constant by the material emissivity coefficient, $\partial T/\partial n$ is the normal derivative of T on the boundary of the workpiece, and T_{amb} is the ambient temperature.

One can also consider an empirical convection law, replacing (2.18) by the condition

$$\lambda \frac{\partial T}{\partial n} + \alpha(T^4 - T_{amb}^4) + \beta(T - T_{amb}) = 0 \tag{2.19}$$

where β is a proportionality coefficient.

The complete model consists in coupling the electromagnetic problem (2.11)–(2.16) with the thermal problem (2.17), (2.18), or (2.19), where we assume that T depends only on the spatial coordinates r and z, and on the time t.

This model includes two kinds of nonlinearities: the first due to the heat source term in the heat equation (2.14), and the second due to the dependence of physical properties of the conductors on the temperature and possibly on the magnetic field.

B. Numerical Solution

We adopted the standard P_1 finite element method for the discretization of equations (2.11) and (2.12), while finite differences in time and standard P_1 finite elements in space were used to solve the heat equation. The mesh used for the thermal problem is the same as the part of the mesh used for the electromagnetic problem inside the conductors. It is worth noticing that the skin effect requires a particularly refined mesh close to the boundary of the conductors. On the other hand, too coarse a mesh inside the conductors would result in an inaccurate solution of the heat equation. Therefore, a reasonable compromise has to be found.

The electromagnetic problem we have to solve is stationary in time, while the heat equation gives rise to an evolutive problem. Due to the different time scale of the two phenomena, we will assume that the solution of the electromagnetic problem is valid on a time interval during which the physical properties of the workpieces do not change too much due to the increase in temperature resulting from the Joule effect. We will then use the result to compute the source term to be plugged into the heat equation. The evolutive heat equation will then be solved using finite differences on the same time interval. The new value of the temperature field thus obtained will be used to update the values of the physical coefficients of the workpieces (ν, σ, ρ, C_p, and λ). This will allow us to proceed to another computation of the magnetic potential, followed by the computation of the temperature field, and so on.

We have developed a numerical simulation code on the basis of the above model. It can deal with any induction heating system having an axisymmetric geometry. Only sinusoidal voltage is allowed, but the restriction on the shape of the voltage does not have a big effect from the energetic point of view. The possibility of having several electric current generators, characterized by different frequencies, voltage amplitudes, and possibly different phases, has been taken into account. The company AMYSA Yverdon S.A. carried out several measurements for different cases of induction heating in axisymmetric

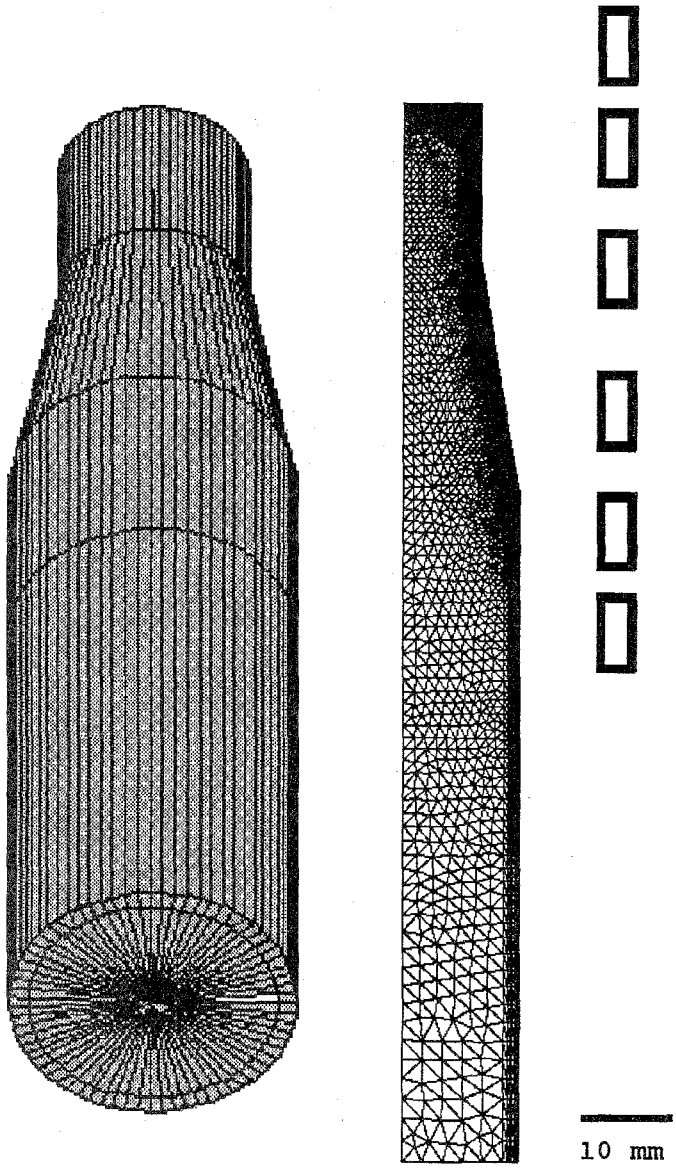

Fig. 3. A three-dimensional representation of the workpiece to be heated. A two-dimensional cross section of the whole induction heating setup.

TABLE I
GEOMETRIC CHARACTERISTICS OF THE EXPERIMENT

total length of the workpiece	135 mm
length of the lower cylindrical part	85 mm
diameter of the lower cylindrical part	30 mm
length of the upper cylindrical part	20 mm
diameter of the upper cylindrical part	20 mm
length of the intermediate part	30 mm
external cross-section of the windings	5 x 10 mm
wall thickness of the windings	1 mm
distance between the two first windings	3 mm
distance between the 2nd and the 3rd winding	5.5 mm
distance between the two middle windings	8 mm
internal diameter of the coil	50 mm
external diameter of the coil	60 mm
distance from the top of the workpiece to the first thermocouple	5 mm
distance from the top of the workpiece to the second thermocouple	35 mm

TABLE II
ELECTRICAL PARAMETERS OF THE EXPERIMENT

total voltage	77 V
active current	40 – 45 A
total current	~ 1293 A
electrical power	13 – 15 kW
capacitance	0.0172 mF
frequency	~ 10 kHz

geometries, in order to get a comparison between numerical simulation and measurements in an industrial environment.

III. Comparison Between Measurements and Numerical Simulation

A. The Measurements

A measurement bank was set up, providing the temperature, the voltage, and optionally the current intensity and the magnetic field in various cases of induction heating processes. A detailed description of this measurement bank can be found in [2].

We consider here the heating of a stainless steel workpiece represented in Fig. 3. The upper part of the workpiece is placed inside a coil consisting of six irregularly spaced windings made of copper. The aim is to obtain as smooth a temperature distribution as possible inside the upper part of the workpiece a couple of seconds after the voltage cutoff, in spite of the corner effect.

The geometric characteristics of the induction heating setup are shown in Table I. It should be mentioned that the coil starts 12.5 mm above the workpiece.

The power supply is a 10 kHz rotating convertor, and the heating time is 25 s. The characteristics of the electric setup are summarized in Table II. The workpiece is made of a nonferromagnetic stainless steel X5CrNi 18/9 (1.4301).

Two thermocouples were spark welded on the surface of the workpiece, at the locations represented in Fig. 4, in order to ensure a good thermal contact. Temperatures as well as voltage were recorded on a calibrated plotter.

B. The Numerical Simulation

The mesh used for the numerical simulation is represented in Fig. 5. We can notice that this mesh is very

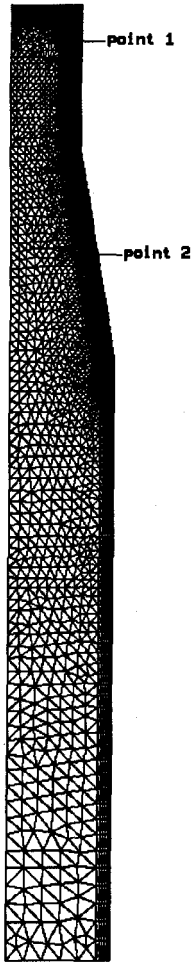

Fig. 4. Location of the measurement points on the workpiece.

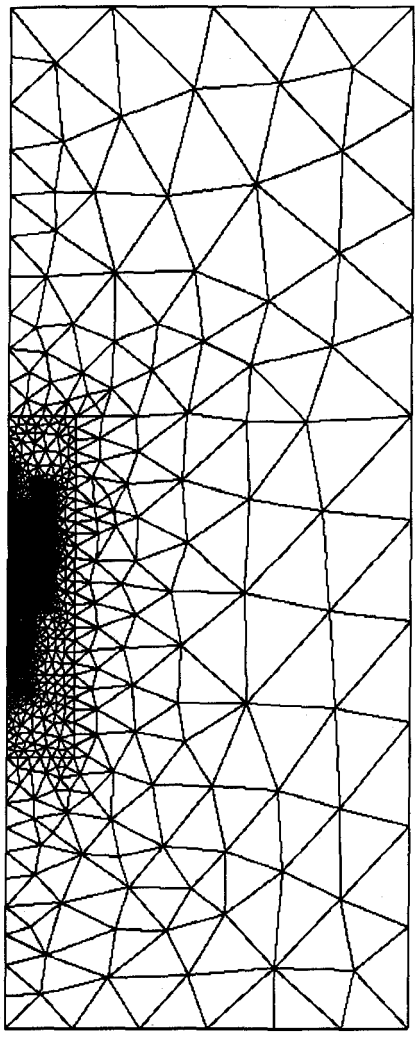

Fig. 5. The mesh used to solve the problem.

refined in the area around the workpiece and the coil, while it becomes gradually coarser close to the boundary of the space area considered. Enlargements of the mesh on the workpiece and the coil can be seen in Figs. 3 and 4.

The timestep used for the computation was 0.1 s. The formulas providing the physical properties of the stainless steel and of the copper used in the numerical simulation are given in [2].

Fig. 6 shows the isotherms at the end of the heating and 7 s later. The isotherms are equally spaced: every 100°C at $t = 25$ s and every 50°C at $t = 32$ s.

Finally, Fig. 7 shows the isolines which correspond to the maximum values in the sinusoidal cycle of the magnetic field inside the workpiece. These isolines are equally spaced: every 2 kA/m for the radial component H_r, and every 10 kA/m for the vertical component H_z. It is worth noticing how the radial component increases close to the upper end of the workpiece and in the area corresponding to the lower extremity of the coil.

C. Comparison and Conclusions

Figs. 8 and 9 below show a comparison between the temperatures obtained by numerical simulation and the temperatures measured during the experiment, at the points shown on Fig. 4.

A generally good agreement is found between experimental results and numerical simulation. However, some sources of experimental and data errors have to be considered, as was extensively discussed in [2]. In this experiment, the difference between the experimental curve and the simulation during the first 10 s can be explained by the fact that voltage cannot be set as a perfect step function. About 2.5 s were necessary to obtain the 77 V steady, and thus the simulation provides higher temperatures at the beginning of the heating. This phenomenon can be observed as a difference in the slope during the first 2.5 s on Figs. 8 and 9. Another cause of discrepancy is the fact that we model a helical coil by an axisymmetric geometry, which is an idealization of the reality. Moreover, the coil was produced without using high precision methods, and the gap between two windings is not constant. The width of this gap cannot be measured very accurately, and numerical simulation shows that moving a winding by a small distance can have a considerable influence on the resulting temperature field. A further factor

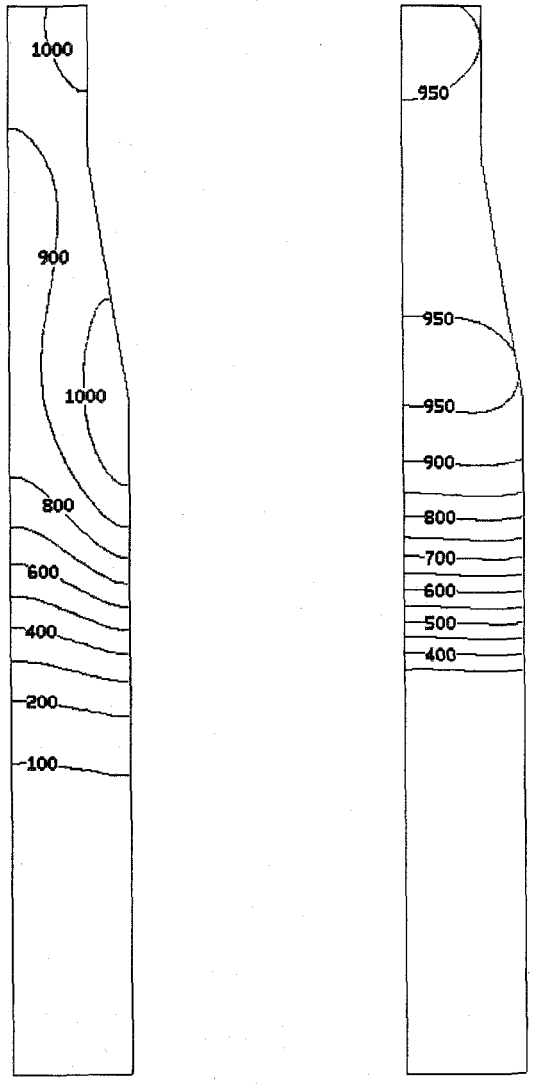

Fig. 6. Isotherms inside the workpiece at $t = 25$ s and at $t = 32$ s.

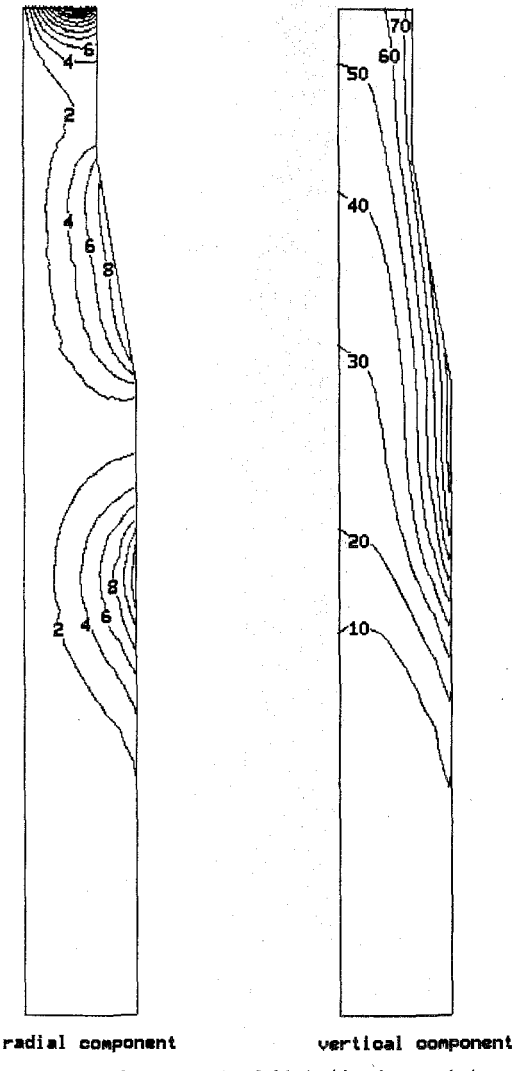

Fig. 7. Isolines of the magnetic field inside the workpiece at $t = 25$ s: modulus of the radial component H_r and of the vertical component H_z (kA/m).

of relevance is whether the workpiece is truly concentric within the coil bore, and aligned on the same axis. Other possible causes for discrepancy lie in the fact that the model itself is an idealization of the reality, and that its solution is obtained using numerical methods whose results can never be exact. However, we do not believe that the latter causes weigh much in the total discrepancy between the experiment and the simulation presented above.

In conclusion, we can affirm that the results presented above are valuable. The case described in [1] and [2] relied upon the assumption that all the induction heating setup is invariant in one dimension. Such a geometry obviously does not exist in reality, but a model based on the invariance assumption provides results that are close to the experiment in the case of long induction heating setups with constant cross section. On the contrary, the model presented in this paper deals with axisymmetric geometries which do exist in the reality. It enables us to tackle intricate workpiece and inductor setups, and puts forward interesting phenomena, such as corner effects, which could not be observed using the two-dimensional

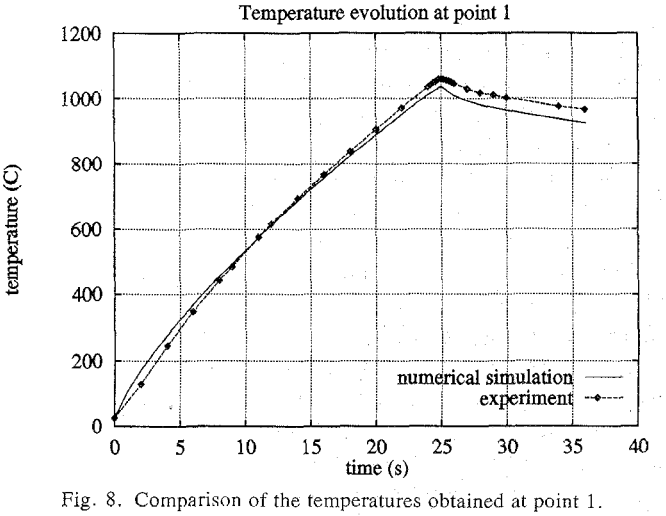

Fig. 8. Comparison of the temperatures obtained at point 1.

code. The benefits of numerical simulation stated in [2] have thus been extended to further situations encountered in industrial practice.

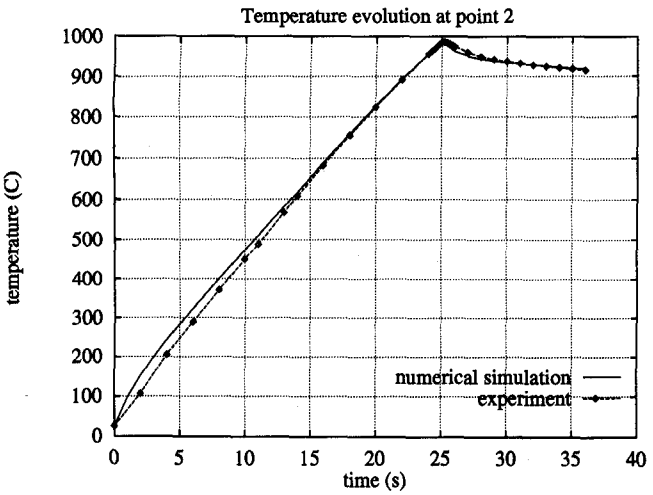

Fig. 9. Comparison of the temperatures obtained at point 2.

REFERENCES

[1] S. Clain, J. Rappaz, M. Swierkosz, and R. Touzani, "Numerical modelling of induction heating for two-dimensional geometries," *Math. Models Methods Appl. Sci.*, vol. 3, no. 6, pp. 805–822, 1993.

[2] C. Chaboudez, S. Clain, R. Glardon, J. Rappaz, M. Swierkosz, and R. Touzani, "Numerical modelling in induction heating of long workpieces," *IEEE Trans. Magn.*, vol. 30, pp. 5026–5037, 1994.

[3] E. J. Davies, *Conduction and Induction Heating*. London: Peregrinus, 1990.

[4] O. Bíró and K. Preis, "Finite element analysis of 3-D eddy currents," *IEEE Trans. Magn.*, vol. 26, pp. 418–423, 1990.

[5] A. Bossavit and J. C. Vérité, "The Trifou code: Solving the 3-D eddy-currents problem by using H as state variable," *IEEE Trans. Magn.*, vol. 19, pp. 2465–2470, 1983.

[6] R. Cardoso Mesquita and J. P. Assumpção Bastos, "3-D finite element solution of induction heating problems with efficient time-stepping," *IEEE Trans. Magn.*, vol. 27, pp. 4065–4068, 1987.

[7] L. R. Egan and E. P. Furlani, "A computer simulation of an induction heating system," *IEEE Trans. Magn.*, vol. 27, pp. 4343–4354, 1991.

[8] A. Gagnoud and I. Leclercq, "Electromagnetic modelling of induction melting devices in cold crucible," *IEEE Trans. Magn.*, vol. 24, pp. 573–575, 1988.

[9] D. Labridis and P. Dokopoulos, "Calculation of eddy current losses in nonlinear ferromagnetic materials," *IEEE Trans. Magn.*, vol. 25, pp. 2665–2669, 1989.

[10] O. Longeot, L. Nicolas, and P. Wendling, "3-D design of an inductor for induction heating using 2D FEM and 3D BIEM modelling," *IEEE Trans. Magn.*, vol. 27, pp. 4004–4007, 1991.

[11] C. Marchand and A. Foggia, "2D finite element program for magnetic induction heating," *IEEE Trans. Magn.*, vol. 19, pp. 2647–2649, 1983.

[12] P. Massé, B. Morel, and T. Breville, "A finite element prediction correction scheme for magneto-thermal coupled problem during Curie transition," *IEEE Trans. Magn.*, vol. 21, pp. 181–183, 1985.

[13] J.-L. Meyer, N. El-Kaddah, and J. Szekely, "A new method for computing electromagnetic force fields in induction furnaces," *IEEE Trans. Magn.*, vol. 23, pp. 1806–1810, 1987.

[14] T. Miyoshi, M. Sumiya, and H. Omori, "Analysis of an induction heating system by the finite element method combined with a boundary integral equation," *IEEE Trans. Magn.*, vol. 23, pp. 1827–1832, 1987.

[15] T. Nakata, N. Takahashi, K. Fujiwara, K. Muramatsu and Z. G. Cheng, "Comparison of various methods for 3-D eddy current analysis," *IEEE Trans. Magn.*, vol. 24, pp. 3159–3161, 1988.

[16] K. Preis, "A contribution to eddy-current calculations in plane and axisymmetric multiconductor systems," *IEEE Trans. Magn.*, vol. 19, pp. 2397–2400, 1983.

[17] M. Ramadan Ahmed, J. D. Lavers, and P. E. Burke, "Boundary element application of induction heating devices with rotational symmetry," *IEEE Trans. Magn.*, vol. 25, pp. 3022–3024, 1989.

[18] T. P. Skoczkowski and M. F. Kalus, "The mathematical model of induction heating of ferromagnetic pipes," *IEEE Trans. Magn.*, vol. 25, pp. 2745–2750, 1989.

[19] J. P. Sturgess and T. W. Preston, "An economic solution for 3-D coupled electromagnetic and thermal eddy current problems," *IEEE Trans. Magn.*, vol. 28, pp. 1267–1269, 1992.

[20] E. J. W. ter Maten and J. B. M. Melissen, "Simulation of inductive heating," *IEEE Trans. Magn.*, vol. 28, pp. 1287–1290, 1992.

[21] A. Quarteroni and A. Vialli, *Numerical Approximation of Partial Differential Equations*, Springer Series in Computational Mathematics 23. Berlin: Springer-Verlag, 1994.